PAPER

A family of mono-, di-, and tetranuclear Dy[III] complexes bearing the ligand 2,6-diacetylpyridine bis(picolinoylhydrazone) and exhibiting slow relaxation of magnetization†

Alexandros S. Armenis, [ID] ‡[a] Georgia P. Bakali, [ID] ‡[a] ChristiAnna L. Brantley,[b] Catherine P. Raptopoulou,[c] Vassilis Psycharis, [ID] [c] Luís Cunha-Silva, [ID] [d] George Christou [ID] [b] and Theocharis C. Stamatatos [ID] ⋆[a,e]

The systematic investigation of the general reaction scheme Dy[III]/X[−]/LH₂, where X[−] = Cl^{−}, CF₃SO₃^{−}, ClO₄^{−}, MeCO₂^{−}, and LH₂ is the pocket-type ligand 2,6-diacetylpyridine bis(picolinoylhydrazone), resulting from the condensation of 2,6-diacetylpyridine with picolinic acid hydrazide, has led to a new family of mono-, di-, and tetranuclear metal complexes of the formulae $[DyCl_2(LH_2)(MeOH)]Cl$ (**1**), $[Dy_2(O_3SCF_3)_2(LH)_2(MeOH)_{1.42}(H_2O)_{0.58}](O_3SCF_3)_2$ (**2**), $[Dy_2(LH)_2(MeOH)_2(H_2O)_2](ClO_4)_4$ (**3**), and $[Dy_4(OH)_2(O_2CMe)_6(L)_2]$ (**4**), respectively. The organic chelate undergoes metal-assisted amide–iminol tautomerism and adopts the neutral zwitterionic, and single- and double-deprotonated forms, respectively, upon coordination with the metal center(s). Interestingly, the different forms of the ligand $LH_2/LH^-/L^{2-}$ act independently as penta-, hexa-, and heptadentate, either as single-chelating or chelating and bridging, thus yielding new Dy[III] compounds of various nuclearities and different magnetic properties. All complexes **1–4** exhibit frequency-dependent, out-of-phase (χ''_M) tails of signals in zero external dc field, characteristic of the onset of quantum tunnelling of magnetization. Attempts to suppress the tunnelling through the application of an external dc field were mostly successful in the case of complex **1**, where entirely visible peaks of χ''_M have been observed and rendered possible the fit of the data to the Arrhenius equation, thus yielding the parameters: U_{eff} = 10.9(1) K and τ_0 = 1.9(1) × 10⁻⁶ s, where U_{eff} is the effective energy barrier for the magnetization reversal and τ_0 is the pre-exponential factor. The combined results demonstrate the ability of pyridyl-bis(acylhydrazone) ligands to yield chemically, structurally, and magnetically interesting compounds through their rich interconversion between various amide–iminol resonance forms.

[a]*Department of Chemistry, University of Patras, 26504 Patras, Greece.
E-mail: thstama@upatras.gr; Tel: +30 2610 997732*
[b]*Department of Chemistry, University of Florida, Gainesville, Florida 32611-7200, USA*
[c]*Institute of Nanoscience and Nanotechnology, NCSR "Demokritos", 15310 Aghia Paraskevi Attikis, Greece*
[d]*LAQV/REQUIMTE & Department of Chemistry and Biochemistry, Faculty of Sciences, University of Porto, 4169-007 Porto, Portugal*
[e]*Institute of Chemical Engineering Sciences, Foundation for Research and Technology – Hellas (FORTH/ICE – HT), Platani, P.O. Box 1414, 26504 Patras, Greece*

Introduction

Single-molecule magnets (SMMs) are coordination compounds which retain their magnetization in the absence of an external magnetic field, and they exhibit frequency- and temperature-dependent out-of-phase (χ''_M) signals and hysteresis loops below a certain temperature, the so-called blocking temperature (T_B).[1] SMMs have been proposed as excellent candidates for potential applications in ultra-high density data storage, quantum computing and spintronics.[2] There are four major classes of SMMs extensively developed to date: polynuclear metal complexes,[3] dinuclear[4] and mononuclear[5] compounds, and organometallic systems.[6]
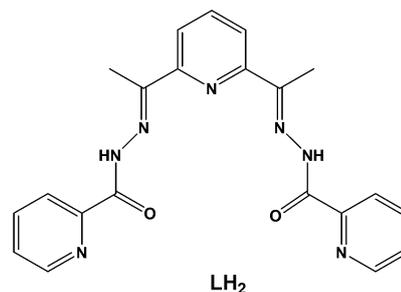
Paramagnetic transition metals in moderate-to-high oxidation states have attracted most of the interest over the past three decades or so, mostly due to their ability to form aesthetically pleasing structures with new motifs and topologies,[7] and fascinating magnetic properties, such as high-spin mole-

cules,[8] SMMs with large energy barriers for magnetization reversal,[9] SMMs with step-like features at periodic fields of the hysteresis loop due to quantum tunnelling of the magnetization (QTM),[10] and molecular magnetic refrigerants.[11] However, the longstanding quest for 3d-metal based SMMs with improved intrinsic properties, such as higher ground-state spin values (S) and larger magnetoanistropies (D), has lagged a bit behind in meeting the needs for some practical applications, which require higher blocking temperatures[12] and more flexible in engineering molecular systems, such as monomers and oligonuclear compounds.[13]

The new era of the field of SMMs has leaned on 4f-metal ions acting as 'protagonists'[14] in the quest for new molecules with enhanced magnetic dynamics and higher blocking temperatures, and hybrid multifunctional materials[15] (*i.e.*, SMMs@graphenes and SMMs@CNTs) with potential applications in the areas of information technology[16] and molecular electronics.[17] In particular, the Dy^{III} ion has had a dominant position over the other lanthanide ions in the pursuit of efficient SMMs.[18] This is mainly due to: (i) the odd number of electrons ($4f^9$), ensuring a bistable ground state (Kramers doublet) irrespective of the symmetry of the ligand field,[19] and (ii) the large spin–orbit coupling and subsequently large magnetic anisotropy, which gives rise to $^6H_{15/2}$ ($^{2S+1}L_J$) multiplets with 16-fold ($2J + 1$) degeneracy; these are further split into $\pm m_j$ sublevels due to the removal of the degeneracy from the surrounding crystal field.[20] The main obstacle towards the preparation of high-performance Dy^{III} SMMs still retains the effect of QTM, which allows the electronic spins to tunnel through the energy barrier following a non-thermally activated pathway.[21] Suppression of the QTM is mainly achieved by either chemical/structural means, such as the synthesis of highly symmetric structures and ideal lanthanide coordination geometries (*i.e* D_{5h} and D_{6h} geometries),[22] or the application of external direct current (dc) fields in alternating current (ac) magnetic dynamics.

Every 'protagonist' – in any demanding field of art and science – to unveil the anticipated skills and performance in action must be surrounded by the appropriate group of "side characters". Organic chelates are key "side characters" and very important players in the field of lanthanide SMMs;[23] they provide thermodynamic stability and crystallinity to the molecular systems, the ability to fine-tune the chemical, structural and electronic properties of the coordination compounds, while the ligand and crystal field effects appear to inherently affect the SMM efficacy, and the quantum tunnelling rates.[24] Hydrazones of the general formula $R_1R_2C{=}N{-}NH$ offer a stable scaffold to chemically manipulate and transform them into pocket-type ligands with high affinity for binding to 4f-metal ions.[25] Along these lines, bis(acylhydrazones) originating from the condensation of 2,6-pyridinedicarbonyl groups and acyl hydrazides appear to be a promising class of polydentate chelates which – upon deliberate R-substitution at the acyl groups – could also act as bridging ligands, facilitating both the formation of mononuclear and polynuclear metal complexes. This is corroborated by the amide–imino tautomerism that

Scheme 1 The structure of the pocket-type ligand 2,6-diacetylpyridine bis(picolinoylhydrazone) (LH$_2$) used in the present work.

these ligands can undergo, thus enhancing their coordinating capabilities and structural versatilities towards various metal ions and topologies, respectively.

In this work, we have employed the ligand 2,6-diacetylpyridine bis(picolinoylhydrazone) (LH$_2$, Scheme 1) in Dy^{III} chemistry, in conjunction with various supporting anions and in the absence or presence of an external base, as a means of preparing new molecular magnetic compounds bearing different resonance forms of the ligand LH$_2$. Indeed, the systematic investigation of the tertiary system $Dy^{III}/X^-/LH_2$, where X^- = Cl^-, $CF_3SO_3^-$, ClO_4^-, and $MeCO_2^-$, has led us to the synthesis, structural, spectroscopic, and magnetic characterization of a family of mono-, di-, and tetranuclear complexes, all exhibiting slow relaxation of the magnetization and containing the neutral zwitterionic, and single- and double-deprotonated forms of the ligand LH$_2$, respectively.
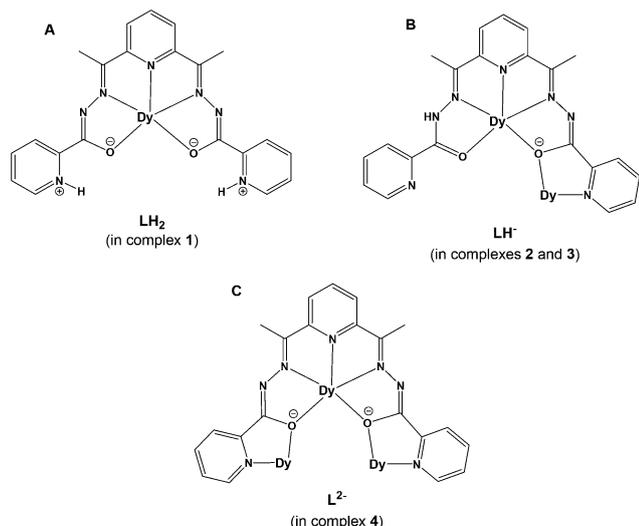
Results and discussion

Synthetic comments and IR characterization

The structural diversity of the reported coordination compounds (**1–4**) is mainly dependent upon the nature of the employed ancillary anions (*i.e.*, Cl^-, $CF_3SO_3^-$, ClO_4^- and $MeCO_2^-$) and the absence or presence of an external organic base (*i.e.*, NEt$_3$). In all cases, the versatility of the pentadentate, pocket-type ligand LH$_2$ towards metal ion-assisted amide–iminol tautomerism has rendered possible the stabilization and crystallization of a family of mono-, di- and tetranuclear Dy^{III} complexes bearing different resonance forms of the neutral zwitterionic LH$_2$ (in complex **1**) and the single- (in complexes **2** and **3**) and double-deprotonated (in complex **4**) forms of LH$^-$ and L^{2-}, respectively (Scheme 2). The crystal structures of **1–4** have allowed us to determine the actual positions of the ligand's H-atoms with respect to the amide or pyridine N-atoms, while the deviations in the carbon–nitrogen and carbon–oxygen bond distances of the amide groups, in conjunction with charge-balance considerations for each of the reported coordination compounds, helped us to further support the assigned resonance forms.

The systematic exploration of the ability of the ligand LH$_2$ to foster the formation of structurally and magnetically inter-

Scheme 2 The crystallographically established coordination modes of the neutral (**A**), single- (**B**) and double-deprotonated (**C**) forms of the ligand LH_2 in complexes **1–4**. The depicted charges on specific N- and O-donor atoms in **A**, **B**, and **C** serve to comprehend the different resonance forms of the ligand LH_2 in its zwitterionic (**A**) or deprotonated (**B** and **C**) forms.

esting Dy^{III} complexes included as a starting point the $DyCl_3$ precursor. The Cl^- ions are well-known for their ability to coordinate to 4f-metal ions, either as terminal monodentate groups or bridging ligands.[26] Therefore, the reaction between $DyCl_3 \cdot 6H_2O$ and LH_2 in a molar ratio of 1 : 2, in a solvent mixture comprising MeOH and $CHCl_3$, afforded yellow-orange prismatic crystals of the mononuclear complex $[DyCl_2(LH_2)(MeOH)]Cl$ (**1**), upon layering with Et_2O, in 65% yield. As noticed from the chemical formula of **1**, the experimental molar ratio of 1 : 2 between $DyCl_3 \cdot 6H_2O$ and LH_2 has turned out to be dissimilar to the stoichiometric 1 : 1. When the same reaction was performed in a 1 : 1 molar ratio between the two reagents, microcrystalline solid (and not single-crystals) of **1** was obtained in yields as high as 85%; the chemical identity of this microcrystalline solid was confirmed by means of IR spectral comparison with the IR spectrum of the original **1**. Furthermore, the reaction solvent mixture of MeOH and $CHCl_3$ was essential for the formation and crystallization of **1**. In the absence of MeOH or its replacement by other alcohols, such as EtOH, n-PrOH or n-BuOH, only amorphous yellow solids were obtained, which were probably mixtures of unreacted LH_2 and unspecified inorganic-based materials (based on the recorded IR spectra). Although $CHCl_3$ does not appear in the crystal structure of **1** as a lattice solvent (*vide infra*), its use as a co-solvent in this reaction scheme was found to yield the best quality single-crystals of **1** compared to similar solvents, such as CH_2Cl_2 and $CHBr_3$.

As a part of the reactivity studies on **1**, we wondered whether it was possible to obtain new Dy^{III}/LH_2 complexes with different resonance forms of LH_2 by omitting the ancillary Cl^- ions and replacing them with anions that have negligible coordination affinity with Dy^{III} centers, such as $CF_3SO_3^-$

and ClO_4^-. Indeed, the 1 : 2 reaction between $Dy(O_3SCF_3)_3$ and the ligand LH_2 in refluxing MeOH (to enhance the solubility of the starting materials) led to yellow prismatic crystals of the dinuclear complex $[Dy_2(O_3SCF_3)_2(LH)_2(MeOH)_{1.42}(H_2O)_{0.58}]$ $(O_3SCF_3)_2$ (**2**), upon layering with Et_2O, in 60% yield. Interestingly, the $CF_3SO_3^-$ ions were found to be a part of both the first- and second-coordination sphere of **2**, acting as terminal monodentate ligands and counterions, respectively. Terminally-bound $CF_3SO_3^-$ ions are rare, albeit of precedence, in Dy^{III} coordination chemistry.[27] In contrast to **2**, the use of $Dy(ClO_4)_3 \cdot xH_2O$ in place of $Dy(O_3SCF_3)_3$, under the same conditions (*i.e.*, Dy^{III}/LH_2 molar ratio, reaction solvent and crystallization process), led to yellow plate-like crystals of the dinuclear complex $[Dy_2(LH)_2(MeOH)_2(H_2O)_2](ClO_4)_4 \cdot 2MeOH$ (**3·2MeOH**) in similar yields (∼55%). In spite of the structural similarities between **2** and **3** in most of their chemical features, the ClO_4^- ions in **3** were found to solely act as counterions, thus allowing H_2O molecules to occupy the remaining coordination sites. It is likely that steric reasons merely facilitate the coordination of $CF_3SO_3^-$ groups (over ClO_4^-) with the Dy^{III} centers. As with many reactions in trivalent lanthanide chemistry, the solution likely contained a mixture of species in equilibrium, and what crystallizes out is determined by the relative solubilities, the nature of counterions, lattice energies, and related factors.[28] In both **2** and **3**, the coordinated organic ligand appears to be in its single-deprotonated form (**B** form in Scheme 2) because of partial amide-to-iminol tautomerism.

Within this context, our last synthetic attempts were focused on studying the effect of an external organic base (*i.e.*, NEt_3) on the organic ligand's resonance forms and subsequently on the stabilization and crystallization of Dy^{III} complexes with new structural motifs. Various reactions within the tertiary $DyX_3/LH_2/NEt_3$ scheme were performed for $X^- = $ halides, NO_3^-, ClO_4^- and $CF_3SO_3^-$, but all failed to produce any crystalline material after many modifications in molar ratios, reaction solvents and crystallization processes. However, when $MeCO_2^-$ ions were employed in the form of $Dy(O_2CMe)_3 \cdot 4H_2O$, and this reacted with LH_2 and NEt_3 in a 2 : 1 : 5 molar ratio and a solvent mixture of MeOH and CH_2Cl_2, a new tetranuclear complex $[Dy_4(OH)_2(O_2CMe)_6(L)_2] \cdot 2CH_2Cl_2$ (**4·2CH_2Cl_2**) was obtained as yellow plate-like crystals (upon layering with Et_2O) in very good yields (∼70%). Complex **4** is very stable under the prevailing basic conditions, and its identity was neither affected by the nature of the external base nor by the $Dy(O_2CMe)_3 : LH_2 : NEt_3$ molar ratio. The same product, but in much lower yields and poorer crystallinities, was obtained when using NMe_3, NPr_3, Me_4NOH, or other similar organic bases. A very large excess of NEt_3 yielded white amorphous solids which were Dy^{III}/oxido/hydroxido mixed species. The reaction solvent MeOH was necessary for the enhancement of the solubility of all starting reagents; reactions in other alcoholic media failed to yield any crystalline material. On the other hand, the use of CH_2Cl_2 as a co-solvent was found to be decisive for the crystallization of **4**; this is also supported by its presence as the crystal lattice solvent in the crystal structure of **4·2CH_2Cl_2**. Finally, the basic conditions

applied within the aforementioned synthetic route have fostered the complete deprotonation of the ligand LH_2 (**C** form in Scheme 2) and contributed towards the stabilization of its iminol form, thus rendering L^{2-} as an unusual heptadentate chelating and bridging ligand within complex **4**.

Tang and coworkers have employed the chemically similar ligand 2,6-(picolinoylhydrazone)pyridine (H_2php), which contains H-atoms in place of the Me-groups in LH_2, for the synthesis of a family of tetranuclear $[Ln_4(\mu_3\text{-}OH)_2(php)_2(O_2CMe)_6(H_2O)_2]$ ($Ln^{III} = Gd^{III}$, Tb^{III}, Dy^{III} and Ho^{III}) complexes with the same structural topology as that of **4** but with dissimilar metric parameters (bond distances and angles) and magnetic properties (*vide infra*).[29] The ligand LH_2 has been previously used by Pelizzi and coworkers for the synthesis and structural characterization of mononuclear Mn^{II},[30] Co^{II},[31] and Sn^{IV} complexes,[32] and a tetranuclear $\{Cu_4^{II}\}$ cluster with a ring-like topology.[33]

The IR spectra of all complexes **1–4** exhibit medium- or strong-intensity broad bands in the region ~3300–3400 cm^{-1}, attributed to the $\nu(OH)$ vibration of the coordinated solvent molecules (MeOH, H_2O, or both) or the OH^- bridging groups (in **4**), and to the $\nu(NH^+)/\nu(NH)$ vibrations of the zwitterionic LH_2 or single-deprotonated LH^- ligands (in **1** or **2/3**).[34] In addition, the medium-to-strong bands in the region ~1600–1650 cm^{-1}, common for all **1–4**, are assigned to the $\nu(C{=}N)$ and pyridyl stretching vibrations.[35] In the IR spectrum of complex **2**, the distinguishment of the bands denoted to the terminally coordinated and uncoordinated triflate ions is clearly unfeasible. Regardless of this drawback, the presence of the triflate ions in the structure of **2** is confirmed by the following bands: (i) a medium broad band at 1288 cm^{-1} attributed to the asymmetric stretching frequency of the SO_3 group, (ii) a medium broad band at 1228 cm^{-1} corresponding to the symmetric stretching frequency of the CF_3 moiety, (iii) a medium band at 1162 cm^{-1} attributed to $\nu_{as}(CF_3)$, (iv) a very strong band at 1031 cm^{-1} corresponding to $\nu_s(SO_3)$, (v) a strong band at 640 cm^{-1} attributed to the bending vibration of the SO_3 group, and (vi) a weak and a medium-strong band at 574 and 516 cm^{-1} corresponding to the $\delta_{as}(CF_3)$ and $\delta_{as}(SO_3)$ vibrations, respectively.[36] The IR spectrum of **3** exhibits a strong band at 1116–1084 cm^{-1} and a medium-intensity band at 630 cm^{-1}, attributable to the IR-active $\nu_3(F_2)[\nu_d(Cl\text{-}O)]$ and $\nu_4(F_2)[\delta_d(OClO)]$ vibrations of the uncoordinated (T_d geometry) ClO_4^- counterions, respectively.[37] Several bands appear in the 1600–1370 cm^{-1} range in the IR spectrum of complex **4**. These are due to contributions from the stretching vibrations of the imino groups, the pyridyl rings and the $MeCO_2^-$ ligands. Since overlap cannot be ruled out, the bands most probably do not represent pure vibrations, and this renders exact assignments and studies of the coordination shifts tentative. The bands at 1568 and 1420 cm^{-1} in the spectrum of **4** are assigned to the $\nu_{as}(CO_2)$ and $\nu_s(CO_2)$ vibrations, respectively, of the acetato ligands, coupled with ring stretching vibrations.[38] The difference Δ, where $\Delta = \nu_{as}(CO_2) - \nu_s(CO_2)$, is 148 cm^{-1}, less than that for NaO_2CMe (164 cm^{-1}), as expected for the bidentate bridging mode of the carboxylate ligation. The asymmetric

and the symmetric carboxylate stretches of the monodentate $MeCO_2^-$ in **4** can be observed at 1545 and 1378 cm^{-1}, respectively, giving a Δ value of 167 cm^{-1}, slightly higher than that of NaO_2CMe; usually higher Δ values as expected for monodentate acetato ligands.[39] The two strong intramolecular hydrogen bonds (*vide infra*) between the uncoordinated carboxylate oxygen and the H-atom of the bridging OH^- group withdraws the electron cloud of the C–O bond closer to the oxygen atom. The C–O bond order slightly decreases which shifts the asymmetric vibration to lower wavenumbers.

The thermal decomposition of complexes **1–4** was studied using thermogravimetric analysis (TGA) techniques under nitrogen. TG data and plots for **1–4** are shown in Fig. S1.† Complex **1** decomposes fast without a clear plateau to progressively lose the coordinated MeOH, the bound and lattice Cl^- ions (in the form of HCl), and the organic chelate LH_2 (from 30 °C to 410 °C). In complex **2**, there is an initial weight loss of ~7% from 30 °C to 130 °C, which perfectly agrees with the loss of four MeOH solvate molecules (calcd: 6.9%). Above 130 °C, the continuous loss of the organic chelates and the triflate ions (in the form of CF_3SO_3H) is observed in the temperature range of 130–400 °C and >400 °C, respectively.[40] The decomposition of complex **3** begins with the loss of lattice MeOH and coordinated MeOH and H_2O molecules to yield a weight loss of ~9.8% up to a temperature of 280 °C (calcd: 9.7%). In temperatures above 280 °C, the gradual loss of the organic chelates and the ClO_4^- ions (in the form of $HClO_4$) is detected. For cluster compound **4**, the loss of the lattice CH_2Cl_2 solvate molecules and the bridging OH^- ions (in the form of H_2O) is obvious in the temperature region 30 °C to 290 °C (experimental weight loss: 9.9%; calcd: 10.1%), while further decomposition is associated with the loss of the coordinated $MeCO_2^-$ groups (in the form of $MeCO_2H$) and the organic chelates.

Description of structures

Selected interatomic distances and angles for complexes **1–4** are listed in Tables S1–S4,† respectively. For the sake of brevity, only important metric parameters will be discussed in the main text. The structure of **1** contains $[DyCl_2(LH_2)(MeOH)]^+$ complex cations and Cl^- counterions in a 1 : 1 ratio. The structure of the $[DyCl_2(LH_2)(MeOH)]^+$ cation of **1** is shown in Fig. 1. It contains a Dy^{III} atom surrounded by an overall neutral, pentadentate chelate LH_2, which is coordinated as its zwitterionic form (**A** in Scheme 2). The pocket-type ligand LH_2 makes use of the two enolate O-atoms (O1 and O2), the two imino N-atoms (N3 and N5) and a pyridyl N-atom (N4) for binding to the Dy^{III} center. The C16–O2 and C6–O1 bond lengths within LH_2 are 1.280(4) and 1.276(4) Å, respectively, further supporting the enolate resonance form of the zwitterionic chelate. Peripheral ligation about the Dy^{III} center is provided by two and one terminally bound Cl^- ions (Cl1 and Cl2) and MeOH (O1M) molecules, respectively. Thus, the metal ion is 8-coordinate, possessing a distorted hexagonal bipyramidal geometry. This was confirmed by the so-called continuous shape measures (CShM) approach of the SHAPE program,[41] which
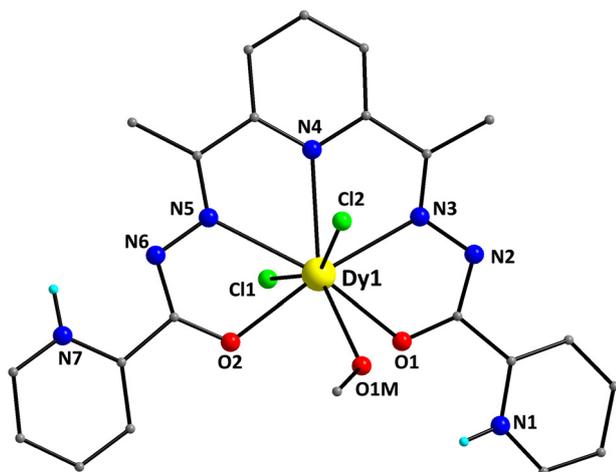
Fig. 1 The structure of the [DyCl₂(LH₂)(MeOH)]⁺ cation that is present in the crystal of **1**. The H-atoms, except those bonded to the pyridyl N-atoms, are omitted for clarity. Color scheme: Dy^{III}, yellow; O, red; N, blue; Cl, green; C, grey; and H, cyan.

allows one to numerically evaluate by how much a particular polyhedron deviates from the ideal shape. The best fit was obtained for the hexagonal bipyramid (CShM value = 5.29; Fig. S2 and Table S5†) with the Cl-atoms occupying the apical positions. Values of CShM larger than 3 correspond to a significant distortion from the ideal geometry. This is also evidenced by the large deviation of the Cl1–Dy1–Cl2 angle (155.6°) from the ideal value of 180.0°. The Dy–O, Dy–Cl and Dy–N bond lengths fall in the range of 2.342(2)–2.486(3), 2.668(8)/2.704(9) and 2.531(3)–2.581(3) Å, and are typical of Dy^{III} complexes containing this set of donor atoms.[42] The bond lengths of Dy^{III} to the deprotonated alkoxido oxygen atoms [2.342(2) and 2.382(2) Å] are noticeably shorter than the distance to the methanol oxygen atom [2.486(3) Å].

The coordinated ligand LH₂ is not strictly planar; this deviation is imposed by the opposite twist of the two pyridyl groups of the picolynoylhydrazone moieties. The two opposite pyridine groups form an angle of 8.9°. As a result, the pyridyl N-atom (N7) gets closer to the uncoordinated imino N-atom (N6), while the other pyridyl N-atom (N1) appears to be closer to the coordinated alkoxido O-atom (O1). The Dy^{III} atom is displaced by 0.25 Å out of the best-mean-equatorial plane that is formed by the coordinated atoms of the ligand LH₂. The intermolecular H-bonding interactions that appeared in the crystal structure of **1** have a pronounced effect on the spatial arrangements of the ligands' atoms (Fig. 2). These interactions involve the coordinated Cl⁻ ion (Cl2) and the uncoordinated pyridinium N–H⁺ moiety (N7),[43] as well as the Cl⁻ counterion (Cl3) and the set of coordinated MeOH solvent and the other uncoordinated pyridinium N–H⁺ moiety (N1). The dimensions of these hydrogen bonds are: N7···Cl2# = 3.130(3) Å, O1M···Cl3 = 3.194(3) Å, and N1···Cl3 = 3.045(3) Å. Interestingly, the hydrogen-bonded monomers of **1** are intermolecularly linked to each other forming {Dy₂} dimers rather than pseudo-polymeric chains of repeating monomers. In addition, the H-bonded
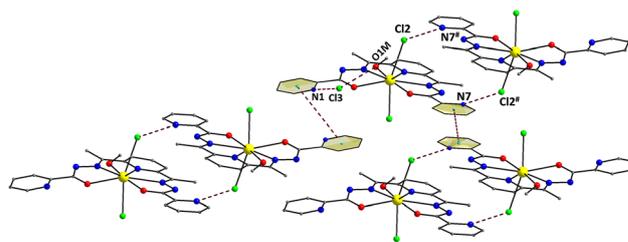

Fig. 2 A portion of the repeating H-bonded dimers in the crystal of **1** and their interactions with their neighboring units through weak π–π stacking interactions. Both H-bonds and π–π stacking interactions are indicated by dashed lines. Symmetry code: # = 2 − x, 2 − y, 1 − z. Color scheme as in Fig. 1.

dimers are only very weakly interacting with their neighboring units *via* π–π stacking interactions between the pyridyl groups of picolynoylhydrazone units of adjacent compounds (centroid-to-centroid distances are 4.694 and 4.979 Å). The shortest intermolecular Dy···Dy separation in the crystal of **1** is 8.230 Å (between the Dy^{III} atoms of the H-bonded dimers).

The structures of the dinuclear complexes [Dy₂(O₃SCF₃)₂(LH)₂(MeOH)$_{1.42}$(H₂O)$_{0.58}$](O₃SCF₃)₂ (**2**) and [Dy₂(LH)₂(MeOH)₂(H₂O)₂](ClO₄)₄·2MeOH (**3·2MeOH**) are very similar to each other, and therefore only that of **3·2MeOH** will be described in detail as a representative example. The major difference between **2** (Fig. S3†) and **3** is the coordination of two terminal triflate ions, one to each Dy^{III} center, in the dicationic **2** over the coordination of two water molecules (in place of the two triflates) in the tetracationic **3**. The most noticeable similarities between the two compounds are (i) the same binding mode of the single-deprotonated ligand LH⁻ (**B** in Scheme 2), (ii) the same {Dy₂(μ-OR)₂}⁴⁺ planar core, and (iii) the same coordination number nine, donor N₄O₅ set and coordination polyhedra of all Dy^{III} atoms.

The structure of **3·2MeOH** contains [Dy₂(LH)₂(MeOH)₂(H₂O)₂]⁴⁺ complex cations, ClO₄⁻ counterions and lattice MeOH solvent molecules in a 1 : 4 : 2 ratio. The structure of the centrosymmetric [Dy₂(LH)₂(MeOH)₂(H₂O)₂]⁴⁺ cation of **3** is shown in Fig. 3. The two Dy^{III} atoms (Dy1 and Dy1′) are linked to each other through the bridging alkoxido O-atoms (O1 and O1′) of two single deprotonated LH⁻ ligands; the latter adopt the η¹:η¹:η¹:η¹:η²:μ binding mode acting as pentadentate chelating/bridging groups. One of the pyridyl groups (N3 and N3′) of each LH⁻ remains unbound and interacts weakly with the lattice MeOH molecules. The C8–O8 and C22–O1 bond lengths within each coordinated LH⁻ are 1.243 and 1.307 Å, respectively, as expected for a keto–enol resonance form of the chelate. Peripheral ligation about the planar {Dy₂(μ-OR)₂}⁴⁺ core (highlighted in Fig. 3) is provided by the chelating part of the LH⁻ ligands, and two terminally bound H₂O (O4 and O4′) and MeOH (O6 and O6′) molecules, one on each Dy^{III} center. The Dy1···Dy1′ separation in **3** is 3.958(4) Å and the Dy1–O1/O1′–Dy1′ angle within its core is 114.6(1)°.

The Dy^{III} atoms are 9-coordinate possessing a distorted muffin-like geometry (CShM value = 2.44; Fig. S4 and Table S6†), with the basal trigonal plane formed by N4, O6,
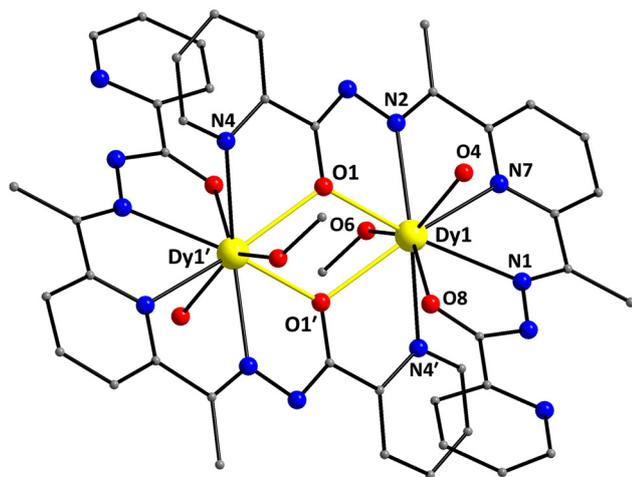
Fig. 3 Partially labelled representation of the $[Dy_2(LH)_2(MeOH)_2(H_2O)_2]^{4+}$ cation that is present in the crystal of **3·2MeOH**, highlighting the $\{Dy_2(\mu\text{-OR})_2\}^{4+}$ core with yellow thick bonds. H atoms are omitted for clarity. Color scheme as in Fig. 1. Symmetry code: (') $1 - x, 1 - y, 1 - z$.
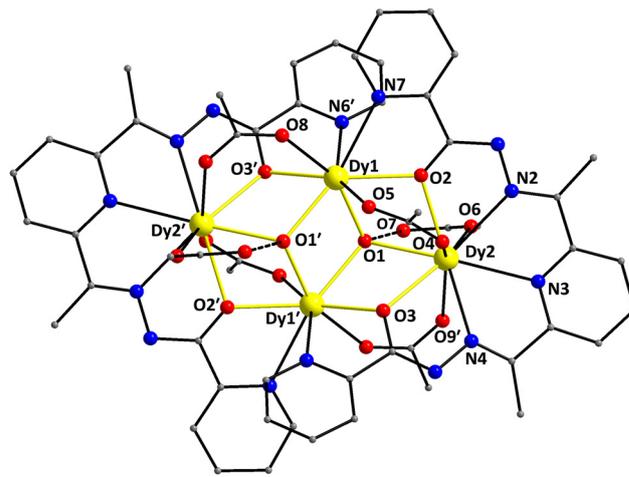

Fig. 4 Partially labelled representation of the $[Dy_4(OH)_2(O_2CMe)_6(L)_2]$ cluster that is present in the crystal of **4·2CH₂Cl₂**, highlighting the $\{Dy_4(\mu_3\text{-OH})_2(\mu\text{-OR})_4\}^{6+}$ core with yellow thick bonds. The dashed lines indicate the intramolecular H-bonds (see the text for the corresponding discussion). H atoms are omitted for clarity. Color scheme as in Fig. 1. Symmetry code: (') $1 - x, 1 - y, 1 - z$.

and O1′ atoms, the equatorial pentagonal plane made of N1, N7, O8, N2, and O1, and the O4 atom occupies the vertex of the muffin.[44] The bond lengths of Dy[III] atoms to the deprotonated alkoxido oxygen atoms [2.315(2) and 2.389(2) Å] are much shorter than the distances to the ketone [2.399(2) Å], methanol [2.406(2) Å], and aqua [2.409(2) Å] oxygen donor atoms. The corresponding CShM value for the 9-coordinate Dy[III] atoms in **2** with a muffin-like geometry is 2.50 (Table S6†).

Finally, there is an extended network of intermolecular H-bonding interactions in the crystal of **3·2MeOH**, which include the coordinated aqua and methanol groups as donors and the ClO_4^- counterions as acceptors (Fig. S5†). These interactions serve to link the dinuclear complexes into a pseudo-1-D chain along the *a*-axis. Their dimensions are O4⋯O7 = 2.804 (7) Å, O4⋯O13 = 2.780(6) Å, and O6⋯O11 = 2.761(5) Å. Furthermore, the lattice MeOH solvate molecules are weakly H-bonded to the ClO_4^- ions and the uncoordinated pyridyl and imino N-atoms of LH⁻, resulting in an overall 2-D hydrogen-bonded network of repeating $\{Dy_2\}$ complexes (Fig. S5†). The shortest intermolecular Dy⋯Dy separation in the crystal of **2** is 9.744 Å.

The structure of **4·2CH₂Cl₂** consists of a tetranuclear $[Dy_4(OH)_2(O_2CMe)_6(L_2)]$ cluster (Fig. 4) and two lattice CH₂Cl₂ molecules; the latter will not be further discussed. Complex **4·2CH₂Cl₂** crystallizes in the triclinic space group $P\bar{1}$ with the $\{Dy_4\}$ molecule lying on an inversion center. The four Dy[III] atoms (Dy1, Dy1′, Dy2, and Dy2′) are located at the four vertices of a defective dicubane, *i.e.* two cubanes sharing a face [Dy(1)O(1)Dy(1′)O(1′)] and each missing one metal vertex. The Dy[III] centers are primarily bridged by two μ_3-OH⁻ (O1 and O1′) and four μ-OR⁻ (O2, O2′, O3, and O3′) groups from two $\eta^1{:}\eta^2{:}\eta^1{:}\eta^1{:}\eta^1{:}\eta^2{:}\eta^1{:}\mu_3$ L²⁻ ligands (**C** in Scheme 2), which are double deprotonated and act as heptadentate chelating and

bridging groups utilizing all available for binding donor atoms. Thus, the core of **4** is $\{Dy_4(\mu_3\text{-OH})_2(\mu\text{-OR})_4\}^{6+}$ (highlighted in Fig. 4), where RO⁻ belongs to L²⁻. Peripheral bridging ligation about the $\{Dy_4\}$ core is provided by four *syn,syn*-$\eta^1{:}\eta^1{:}\mu$ $MeCO_2^-$ groups, while terminal ligation is granted by two η^1 $MeCO_2^-$ and the chelating part of L²⁻. The dangling acetate O atoms (O7 and O7′) are intramolecularly H-bonded to the μ_3-OH⁻ groups [O1⋯O7 = 2.728(6) Å]. The bridging OH⁻ groups are displaced by 0.839 Å from the corresponding Dy₃ best-mean-planes towards the monodentate acetate groups.

The two edge-sharing $\{Dy_3\}$ triangles in **4** form a dihedral angle of 142.9° between them. The triangular $\{Dy_3\}$ units are near isosceles within the 3σ-criterion; the Dy1⋯Dy1′ and Dy1⋯Dy2 distances are 3.720(5) and 3.793(4) Å, respectively, while the Dy1⋯Dy2′ separation is 3.946(5) Å. Complex **4** can alternatively be described as containing a 'butterfly' of Dy[III] sites with the 'body' of the 'butterfly' (Dy1 and Dy1′) bridged by the O-atoms of two μ_3-OH⁻ groups; these O atoms also bridge two Dy[III] 'wing-tip' sites (Dy2 and Dy2′). The long 'wing-tip' Dy2⋯Dy2′ separation is 6.788(5) Å. Each of the four edges of the closed-type 'butterfly' is bridged by a μ-OR group from the chelate ligands L²⁻ and a $\eta^1{:}\eta^1{:}\mu$ $MeCO_2^-$ group.

The Dy1/Dy1′ and Dy2/Dy2′ atoms in **4** are 8- and 9-coordinate, possessing distorted biaugmented trigonal prismatic (CShM value = 2.22) and muffin-like geometries (CShM value = 3.16), respectively (Fig. 5 and Table S7†). The biaugmented trigonal prismatic geometry (Dy1 and Dy1′) is a trigonal prism capped on two of the three rectangular faces;[45] the latter faces consist of the atoms O5/O8/O3/O1, O8/O3/N6/N7, and O5/O1/N6/N7, while the capping atoms are the O2 and O1′. In the muffin-like geometry of Dy2 (and Dy2′), the basal trigonal plane is formed by O2, O4, and N2 atoms, the equatorial pentagonal plane is made of O6, O1, O3, N4, and N3, and the O9′
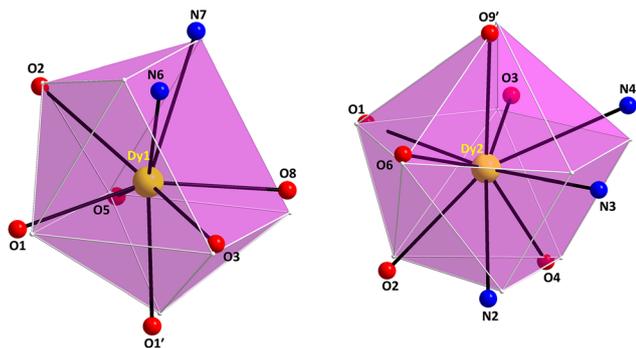
Fig. 5 The biaugmented trigonal prism (left) and muffin (right) co-ordination polyhedra of the Dy^{III} centers in complex **4**·CH$_2$Cl$_2$ with the corresponding atom labelling scheme as discussed in the text. The smaller white spheres define the vertices of the corresponding ideal polyhedra. Color scheme as in Fig. 1. Symmetry code: (') 1 − x, 1 − y, 1 − z.
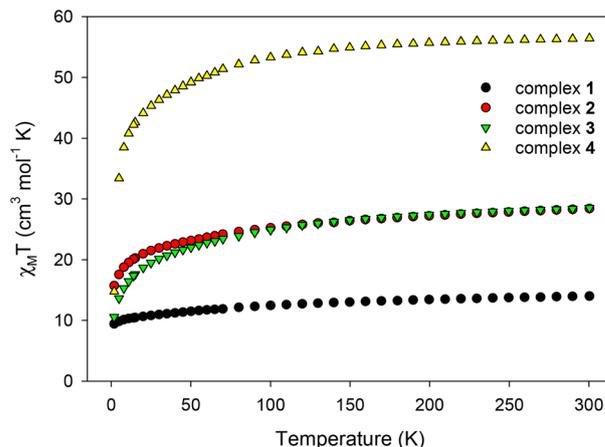

Fig. 6 Temperature dependence of the $\chi_M T$ products for complexes **1–4** at 0.1 T.

atom occupies the vertex of the muffin; the Dy2–O9' distance of 2.370(5) Å is the shortest one within the muffin polyhedron.

From a supramolecular point of view, the {Dy$_4$} clusters in the crystal of **4**·2CH$_2$Cl$_2$ are nicely packed with each other through an extended network of intermolecular π–π stacking interactions between the pyridyl groups of the L^{2-} ligands, thus forming 2-D sheets with cavities, in which the lattice CH$_2$Cl$_2$ solvate molecules are resided (Fig. S6†). The centroid-to-centroid distances of the π–π stacking interactions are 3.409 and 3.497 Å along the a- and b-axis, respectively. The shortest intermolecular Dy⋯Dy separation in the crystal of **4**·2CH$_2$Cl$_2$ is 9.296 Å.

Although there are many tetranuclear {Dy$_4$} clusters reported in the literature, possessing the {Dy$_4$(μ$_3$-OH)$_2$(μ-OR)$_4$}$^{6+}$ 'butter-fly'-like core,[46] complex **4** is structurally more reminiscent to the complex [Dy$_4$(μ$_3$-OH)$_2$(php)$_2$(O$_2$CMe)$_6$(H$_2$O)$_2$], featuring the dianion of 2,6-(picolinoylhydrazone)pyridine (H$_2$php).[29] However, a closer inspection of the two structural motifs reveals some noticeable differences, which comprise no co-ordinated aqua ligands in **4**, the different binding modes of the acetate groups, and the dissimilar coordination numbers and geometries of the Dy^{III} centers (9- and 10-coordinate in the {Dy$_4$}/php^{2-} cluster). This illustrates further the rich coordination and structural chemistry of bis(acylhydrazone) ligands, even in cases of ligands with many chemical similarities between them.

Magnetic susceptibility studies

Direct current (dc) magnetic susceptibility measurements were performed on microcrystalline samples of **1–4** in the 1.8–300 K range under an applied magnetic field of 0.1 T (Fig. 6). Note that the samples used for the magnetic studies have been readily analyzed by elemental analyses, which confirmed their chemical purity and allowed for the accurate determination of their exact molecular weights. The room-temperature $\chi_M T$ values of 13.98 (**1**), 28.40 (**2**), 28.50 (**3**), and 56.45 (**4**) cm^3 K mol^{-1} are very close to the theoretical values of 14.17 (**1**), 28.34

(**2** and **3**), and 56.68 (**4**) cm^3 K mol^{-1} for one, two and four non-interacting Dy^{III} ions (^{6}H$_{15/2}$, S = 5/2, L = 5 and g = 4/3), respectively.[47] For all complexes, $\chi_M T$ steadily decreases on cooling until ∼5 K, and then more sharply, reaching values of 9.40 (**1**), 15.70 (**2**), 10.54 (**3**), and 14.73 (**4**) cm^3 K mol^{-1} at 1.8 K. The abrupt decline of $\chi_M T$ for all complexes as the temperature is lowered is primarily due to the depopulation of the m$_j$ sublevels of the ground J state,[48] and possibly the presence of some weak intramolecular antiferromagnetic interactions between the Dy^{III} ions (in **2**, **3**, and **4**).[14,49] The most notice-able, low temperature decrease of $\chi_M T$ is that observed for the tetranuclear compound **4**; this could be attributed to a larger separation between the ground and excited m$_j$ states and a greater magnetic anisotropy (*vide infra*).[50] Reduced magnetiza-tion ($M/N\mu_B$ *vs.* H/T) studies were also performed (Fig. S7†) for all four complexes in various dc fields (0.1–7.0 T) and low temperatures (1.8–10.0 K). In all cases, the isofield lines do not superimpose into a single master curve, suggesting the pres-ence of unquenched magnetic anisotropy. This is further sup-ported by the fact that the magnetization values at the maximum applied fields (∼5$N\mu_B$ in **1**, ∼11$N\mu_B$ in **2**, ∼10$N\mu_B$ in **3**, and ∼20$N\mu_B$ in **4**) are significantly lower than the expected values for one (10$N\mu_B$), two (20$N\mu_B$), and four (40$N\mu_B$) isolated Dy^{III} centers.[51]

The evaluation of the magnetic dynamics of complexes **1–4** was probed by alternating current (ac) magnetic susceptibility measurements at zero applied dc field, under a weak ac field of 3.5 G at oscillation frequencies of 50–1500 Hz. The common feature of all compounds is the appearance of frequency-dependent tails of peaks in the out-of-phase (χ''_M) suscepti-bilities *vs.* T plots at temperatures below ∼10 (for **1–3**) and ∼6 K (for **4**), suggesting the onset of slow magnetization relax-ation and SMM behavior (Fig. 7). These broad tails of signals are clear indications of fast quantum tunneling of magnetiza-tion (QTM), and consequently small energy barriers for mag-netization reversal. This is a common phenomenon in mono-, di- and polynuclear 4f-SMMs with low-symmetry structures, in
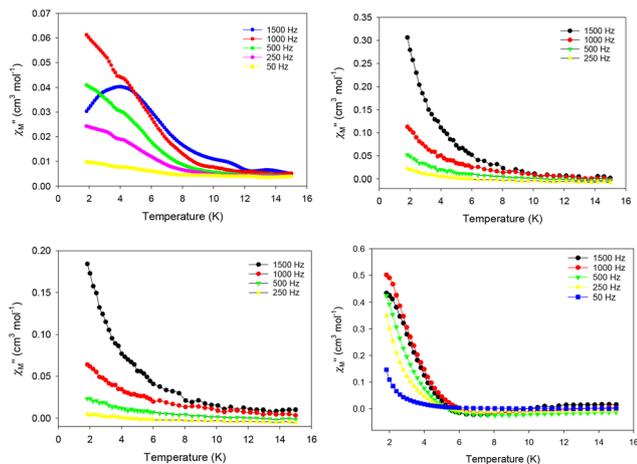
Fig. 7 Temperature dependence of the out-of-phase (χ''_M) ac magnetic susceptibilities in zero dc field for **1** (top left), **2** (top right), **3** (bottom left), and **4** (bottom right) measured in a 3.5 G ac field oscillating at frequencies of 50–1500 Hz. The solid lines are guides only.

which the metal centers adopt various distorted coordination geometries with a random orientation of their single-ion anisotropies, with respect to the molecular easy-axis.[52]

In particular, for Kramers ions such as Dy[III] in the majority of coordination environments, the presence of easy-axis anisotropy, and dipole–dipole and hyperfine interactions allows the mixing of the individual Dy[III] ground states in zero dc field, thus amplifying the QTM mechanism over the thermally-assisted relaxation processes (Orbach and Raman).[53] Although the hexagonal bipyramidal geometry of the Dy[III] center is an appealing coordination environment for the preparation of air-stable mononuclear SMMs with large energy barriers,[54] this turned out not to be the case for **1**. This is readily explained on the basis of the large deviation of Dy[III] in **1** from the ideal D_{6h} geometry, the orientation of the hard- and soft-donor ligands around the equatorial plane and the axial positions, and subsequently the operating crystal field effects which do not allow for specific terms of the crystal field Hamiltonian (*i.e.*, the B_k^q term), responsible for the mitigation of QTM, to vanish and ideally quench the fast relaxation of the magnetization.[55] A search in the Cambridge Structural Database (CSD) revealed the absence of mononuclear Dy[III] complexes bearing a $N_3O_3Cl_2$ set of donor atoms. The closest environment to that of **1** can be resembled by the 8-coordinate compounds [DyCl(bpy)$_2$(H$_2$O)$_3$]Cl$_2$ (DyN$_4$O$_3$Cl chromophore) and [DyCl(terpy)(H$_2$O)$_4$]Cl$_2$ (DyN$_3$O$_4$Cl chromophore),[56] in which no magnetic data were reported (bpy and terpy are the ligands 2,2′-bipyridine and 2,2′:6′,2″-terpyridine, respectively), while no results were derived from the search of the DyN$_4$O$_2$Cl$_2$ and DyN$_2$O$_4$Cl$_2$ chromophores.

To tackle the dominant QTM pathway, a common strategy is the application of an external dc field in ac magnetometry, targeting the shift of the χ''_M signals to higher temperatures and the observation of entirely visible peaks. Indeed, the application of an external dc field of 0.1 T in the ac measurements

of **1** revealed clear, frequency-dependent out-of-phase, χ''_M, signals in the temperature range of 1.8–4 K (Fig. 8, top), which is indicative of a thermally-assisted relaxation process. The χ''_M *vs. T* data were used to construct an Arrhenius-type plot of $\ln(\tau)$ *vs.* $1/T$, where τ is the relaxation time as deduced from the equation: $\tau = (2\pi f)^{-1}$ for every ac frequency f, and T is the temperature value (peak maximum) derived from the fit of χ''_M signals. The linearity of the $\ln(\tau)$ *vs.* $1/T$ plot (Fig. 8, bottom) allowed us to fit the data according to the Arrhenius law [$\ln(\tau)$ = $\ln(\tau_0) + U_{eff}/k_B T$]; the fit yielded a small effective energy barrier, U_{eff}, of 10.9(1) K and a pre-exponential factor, τ_0, of 1.9(1) $\times$ 10^{-6} s.

Unfortunately, the application of an external dc field did not alter the ac profiles of complexes **2**, **3**, and **4**, and no peaks of signals were obtained, suggesting that QTM is still the most dominating mechanism for the magnetization relaxation of these compounds. We have thus focused on quantifying the expectedly small energy barriers of **2**–**4** using the ac data at zero dc field. Assuming that the magnetization relaxation has only one characteristic time that corresponds to a Debye relaxation process, the SMM parameters can be deduced by applying the Kramers–Kronig equations,[57] which result in the combined eqn (1):

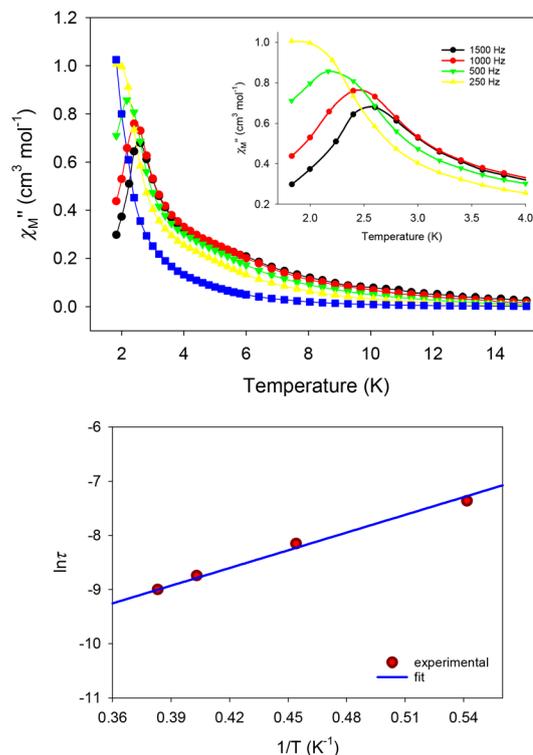$$\ln(\chi''/\chi') = \ln(\omega\tau_0) + U_{eff}/k_B T, \qquad (1)$$

Fig. 8 (Top) χ''_M *vs. T* plot for **1** at 0.1 T dc field, measured under a 3.5 G ac field oscillating at the indicated frequencies; the inset highlights the peak maxima obtained at the indicated temperature region. (Bottom) Arrhenius-type plot of $\ln \tau$ *vs.* $1/T$ for **1**, constructed from the χ''_M *vs. T* data under the applied dc field of 0.1 T; the solid blue line represents the fit that gave the U_{eff} and τ_0 values mentioned in the text.
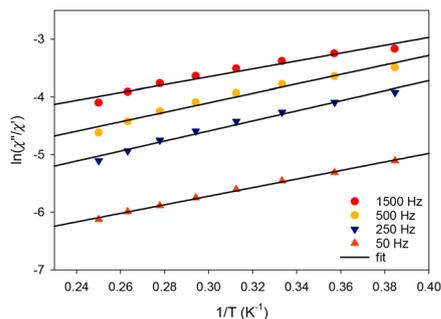
Fig. 9 Debye plots of complex **4** in the temperature range 1.8–5.2 K for the indicated ac frequencies. The solid lines correspond to the fit of the data by applying eqn (1); see the text for the fit parameters.

where ω is the angular frequency, τ_0 is the pre-exponential factor, U_{eff} is the effective energy barrier for the magnetization reversal, and k_B is Boltzmann's constant. The best-fit parameters obtained for complexes **2** and **3** (Fig. S8†) were $U_{eff} =$ 1.2(1) K and $\tau_0 = 1.4(2) \times 10^{-6}$ s, and $U_{eff} = 1.4(2)$ K and $\tau_0 = 1.8(2) \times 10^{-6}$ s, respectively. The resulting energy barriers are very small, and thus a thermally-assisted Orbach process may be discarded as an operative mechanism for the magnetization relaxation processes in dinuclear complexes **2** and **3**.[58] Such a fast relaxation process has been previously seen in many similar dinuclear {Dy$_2$} clusters featuring the {Dy$_2$(μ-OR)$_2$}$^{4+}$ core.[59]

The corresponding best-fit parameters for the tetranuclear complex **4** (Fig. 9) were $U_{eff} = 7.8(2)$ K and $\tau_0 = 6.1(2) \times 10^{-7}$ s. The structurally similar complex [Dy$_4$(μ_3-OH)$_2$(php)$_2$(O$_2$CMe)$_6$(H$_2$O)$_2$] does not exhibit any out-of-phase ac signals in the absence of an external dc field, but it is a field (dc = 0.12 T)-induced SMM with two relaxation phases corresponding to the high- and low-frequency regions. No U_{eff} and τ_0 parameters were reported for this compound. The differences in the magnetic dynamics of **4** over the {Dy$_4$}/php^{2-} cluster[29] can be tentatively assigned to the dissimilar coordination numbers and geometries of the individual Dy^{III} ions, as well as the intra- and intermolecular structural and supramolecular variations, respectively.

Concluding comments and perspectives

In conclusion, we have herein reported a family of mono-, di-, and tetranuclear Dy^{III} complexes resulting from the structural flexibility of the pocket-type ligand 2,6-diacetylpyridine bis(picolinoylhydrazone) (LH$_2$) under different synthetic conditions, including the use of various ancillary anions with coordinating or non-coordinating ability, in the absence or presence of an external base. As a result of this systematic study, the organic versatile ligand LH$_2$ was proved to act as (i) pentadentate chelate under its neutral, zwitterionic form in the mononuclear complex **1**, (ii) hexadentate chelating and

bridging ligand under its single-deprotonated, amide–iminol tautomerism form in the dinuclear compounds **2** and **3**, and (iii) heptadentate chelating and bis-bridging ligand under its double-deprotonated, iminol form in the tetranuclear cluster **4**. From a magnetism viewpoint, all the reported compounds exhibit slow magnetization relaxation under zero external dc field albeit with small energy barriers, because of the efficient quantum tunneling of the magnetization between the lowest m$_j$ sublevels of the ground J state. Attempts to switch-off the tunnelling through the application of an external dc field, all failed to significantly improve the SMM properties. Only the mononuclear complex **1**, which possesses a very distorted D_{6h} geometry, showed entirely visible out-of-phase ac signals under a dc field of 0.1 T, but still the energy barrier was significantly small when compared to the huge energy barriers reported for hexagonal bipyramidal Dy^{III} monomers with ideal D_{6h} geometry.

Work in progress includes the chemical modulation of the coordination geometry of **1** by either removing the coordinating MeOH solvate molecule and replacing the axial Cl$^-$ ions with strongly binding anions, such as Ph$_3$SiO$^-$ or derivatives of phenolate groups, or replacing the MeOH molecule of the equatorial plane with bulkier coordinating solvents, as a means of exerting a "chemical pressure" to the system towards adopting a closer to the ideal D_{6h} geometry. These short-term objectives aim at the synthesis of air-stable, mononuclear single-molecule magnets with large energy barriers for magnetization reversal.

Experimental section

General, physical measurements and spectroscopic studies

All manipulations were performed under aerobic conditions using materials (reagent grade) and solvents as received. The organic ligand LH$_2$ was prepared and characterized according to the literature methods described elsewhere.[60] The reaction is a simple hydrazone condensation of one equivalent of 2,6-diacetylpyridine with two equivalents of picolinic acid hydrazide in refluxing MeOH (yellowish solid; 90% isolated yield). Elemental analyses were performed by the microanalytical service of the University of Patras. FT-IR spectra (4000–400 cm^{-1}) were recorded using a Thermo Scientific Nicolet iS20 spectrometer with samples prepared as KBr pellets. Thermogravimetric analysis (TGA) was conducted on a Labys TG (Setaram Instrumentation) under N$_2$ flow from 25 °C to 600–800 °C with a heating rate of 10 °C min^{-1}. Direct current (dc) and alternating current (ac) magnetic susceptibility studies were performed at the University of Florida Chemistry Department on a Quantum Design MPMS-XL SQUID susceptometer equipped with a 7 T magnet and operating in the 1.8–400 K range. Samples were embedded in solid eicosane to prevent torquing. Alternating current magnetic susceptibility measurements were performed in an oscillating ac field of 3.5 G and either a zero or an external dc field when required. Oscillation frequencies were in the 50–1000 Hz

range. Pascal's constants were used to estimate the diamagnetic correction, which was subtracted from the experimental susceptibility to give molar paramagnetic susceptibility (χ_M).[61]

Synthetic details

Preparation of [DyCl$_2$(LH$_2$)(MeOH)]Cl (1). Solid DyCl$_3$·6H$_2$O (0.038 g, 0.10 mmol) was added to a stirred yellowish suspension of LH$_2$ (0.080 g, 0.20 mmol) in a solvent mixture comprising MeOH (8 mL) and CHCl$_3$ (2 mL). The resulting yellow solution was stirred for a further 20 min, until all solids dissolved, then filtered, and the filtrate was layered with Et$_2$O (20 mL). Slow mixing gave after 3 days yellow-orange prismatic crystals of **1**. The crystals were collected by filtration, washed with cold MeOH (2 × 2 mL) and Et$_2$O (3 × 2 mL), and dried in air. The yield was ∼65% (based on Dy). The product was analyzed satisfactorily as lattice solvent-free, *i.e.* as **1**. Anal. calcd for C$_{22}$H$_{23}$N$_7$O$_3$DyCl$_3$: C, 37.62; H, 3.30; N, 13.96%. Found: C, 37.53; H, 3.19; N, 14.03%. IR bands (KBr, cm^{-1}): 3376sb, 3050m, 1625s, 1564m, 1522vs, 1458m, 1431m, 1373m, 1333w, 1302m, 1261m, 1207m, 1164m, 1087w, 1044w, 1002m, 911m, 820m, 751m, 700m, 679w, 620m, 524w, 435m.

Preparation of [Dy$_2$(O$_3$SCF$_3$)$_2$(LH)$_2$(MeOH)$_{1.42}$(H$_2$O)$_{0.58}$] (O$_3$SCF$_3$)$_2$ (2). Solid Dy(O$_3$SCF$_3$)$_3$ (0.061 g, 0.10 mmol) was added to a stirred yellowish suspension of LH$_2$ (0.080 g, 0.20 mmol) in MeOH (12 mL). The resulting yellow suspension was refluxed for 1 h, during which time all solids dissolved, and the solution turned intense yellow and clear. The latter solution was filtered, and the filtrate was layered with Et$_2$O (20 mL). Slow mixing gave after 7 days yellow prismatic crystals of **2**. The crystals were collected by filtration, washed with cold MeOH (2 × 2 mL) and Et$_2$O (3 × 2 mL), and dried in air. The yield was ∼60% (based on Dy). The product was analyzed satisfactorily as lattice solvent-free, *i.e.* as **2**. Anal. calcd for C$_{47.42}$H$_{42.84}$N$_{14}$O$_{18}$Dy$_2$F$_{12}$S$_4$: C, 32.03; H, 2.43; N, 11.03%. Found: C, 32.13; H, 2.37; N, 11.05%. IR bands (KBr, cm^{-1}): 3305mb, 1743m, 1656m, 1594w, 1568w, 1538m, 1511m, 1434m, 1362m, 1288mb, 1162m, 1093w, 1031vs, 911m, 817m, 755s, 640s, 574m, 516m, 429mb.

Preparation of [Dy$_2$(LH)$_2$(MeOH)$_2$(H$_2$O)$_2$](ClO$_4$)$_4$·2MeOH (3·2MeOH). A colourless solution of Dy(ClO$_4$)$_3$·xH$_2$O (0.066 mL, 0.10 mmol) in MeOH (5 mL) was added to a stirred yellowish suspension of LH$_2$ (0.080 g, 0.20 mmol) in the same solvent (10 mL). The resulting yellow solution was stirred for a further 20 min, filtered and the filtrate was layered with Et$_2$O (30 mL). Slow mixing gave after 5 days yellow plate-like crystals of **3·2MeOH**. The crystals were collected by filtration, washed with cold MeOH (2 × 2 mL) and Et$_2$O (3 × 2 mL), and dried in air. The yield was ∼55% (based on Dy). The product was analyzed satisfactorily as lattice MeOH-free, *i.e.* as **3**. Anal. calcd for C$_{44}$H$_{48}$N$_{14}$O$_{24}$Dy$_2$Cl$_4$: C, 32.55; H, 2.98; N, 12.08%. Found: C, 32.53; H, 2.79; N, 12.13%. IR bands (KBr, cm^{-1}): 3402sb, 2926w, 1642m, 1622m, 1590m, 1564m, 1534m, 1474m, 1430m, 1358m, 1292w, 1260w, 1146s, 1116vs, 1084vs, 1010m, 910w, 818m, 752m, 698w, 676w, 630m, 552mb, 458w.

Preparation of [Dy$_4$(OH)$_2$(O$_2$CMe)$_6$(L)$_2$]·2CH$_2$Cl$_2$ (4·2CH$_2$Cl$_2$). Solid Dy(O$_2$CMe)$_3$·4H$_2$O (0.082 g, 0.20 mmol) was added to a stirred yellowish suspension of LH$_2$ (0.040 g, 0.10 mmol) in a solvent mixture comprising MeOH (7 mL) and CH$_2$Cl$_2$ (7 mL). To the resulting yellow solution, NEt$_3$ (0.070 mL, 0.50 mmol) was added, and the stirring of the solution was maintained for a further 1 h without any noticeable colour change. The final yellow solution was filtered, and the filtrate was layered with Et$_2$O (30 mL). Slow mixing gave after 2 days yellow plate-like crystals of **4·2CH$_2$Cl$_2$**. The crystals were collected by filtration, washed with cold CH$_2$Cl$_2$ (2 × 3 mL) and Et$_2$O (3 × 2 mL), and dried in air. The yield was ∼70% (based on Dy). The product was analyzed satisfactorily as lattice CH$_2$Cl$_2$-free, *i.e.* as **4**. Anal. calcd for C$_{54}$H$_{54}$N$_{14}$O$_{18}$Dy$_4$: C, 35.31; H, 2.96; N, 10.67%. Found: C, 35.43; H, 3.11; N, 10.53%. IR bands (KBr, cm^{-1}): 3417mb, 2922w, 1568vs, 1545vs, 1471m, 1420s, 1378s, 1289w, 1255m, 1178m, 1133w, 1040m, 1010m, 979w, 913w, 812m, 755m, 701m, 642m, 566w, 502w, 453m.

Single-crystal X-ray crystallography

Yellow crystals (0.32 × 0.18 × 0.15 mm) of **1** and **2** (0.20 × 0.17 × 0.14 mm) were taken directly from the mother liquor and immediately cooled to 180 and 190 K, respectively. X-ray diffraction data were collected on a Rigaku R-AXIS SPIDER Image Plate diffractometer using graphite-monochromated Mo Kα (λ = 0.71073 Å) radiation. Data collection (ω-scans) and processing (cell refinement, data reduction and empirical absorption correction) were performed using the CrystalClear program package.[62] The structures of **1** and **2** were solved by direct methods using SHELXS ver. 2013/1[63] and refined by full-matrix least-squares techniques on F^2 with SHELXL ver. 2014/6.[64] H atoms were either located by difference maps and refined isotropically or were introduced at calculated positions as riding on their respective bonded atoms. All non-H atoms were refined anisotropically. The SQUEEZE procedure[65] was used for the analysis of the structures of **1** and **2**; in both **1** and **2** the unit cells contained two methanol solvent molecules, which have been treated as a diffuse contribution to the overall scattering without specific atom positions. With respect to compound **2**, the site labeled as O1M is occupied by two ligands; the estimated value for the occupancy of this site by a methanol molecule is 0.71(1) and by a water one 0.29(1). Sites O1M are shared by oxygen atoms of both the hydroxyl group of methanol and water solvate ligands. Also, the sites of H1MB hydrogen atoms are occupied by one hydrogen atom of the water ligand and the hydrogen atom from the hydroxyl group of methanol ligands. The sites H1MA are occupied only by the second hydrogen atom of water ligands with an estimated occupancy of 0.29(1). C24 atom sites and the respective hydrogen atoms of the methyl group have 0.71(1) occupancy. The description of disorder of this model at these sites is completed by considering the presence of methanol lattice molecules at the sites O25 and C26 with an occupancy of 0.29(1). Also, the coordinated triflate anions occupy two sites with 0.902(3) and 0.098(3) occupancies.

Single-crystal X-ray diffraction data of complex **3·2MeOH** were collected on a yellow plate-like crystal (0.06 × 0.05 ×

0.04 mm) using a Rigaku Oxford Diffraction XtaLAB Synergy diffractometer equipped with a HyPix-6000HE area detector at 173 K and utilizing Cu Kα (λ = 1.54184 Å) radiation from a PhotonJet micro-focus X-ray source. The structure was solved using SHELXT ver. 2018/2 and refined by full-matrix least-squares techniques against $F_o{}^2$ using the SHELXL ver. 2018/3 program[63] through the OLEX2 interface.[66] The non-hydrogen atoms were successfully refined using anisotropic displacement parameters, and hydrogen atoms bonded to the carbon, nitrogen and oxygen atoms of the ligands were placed at their idealized positions using appropriate HFIX instructions in SHELXL. All these atoms were included in subsequent refinement cycles in riding-motion approximation with isotropic thermal displacement parameters (U_{iso}) fixed at 1.2 or 1.5 × U_{eq} of the relative atom.

A yellow crystal (0.20 × 0.07 × 0.07 mm) of $4\cdot2CH_2Cl_2$ was mounted on a CryoLoop with the assistance of a stereomicroscope.[67] Diffraction data were collected on a Bruker D8 diffractometer (Mo Kα graphite-monochromated radiation, λ = 0.71073 Å) with the acquisition controlled by the APEX2 software package.[68] The temperature of data acquisition was 150(2) K, and it was set up with a cryosystem by the Oxford Cryosystems Series 700. Images were processed with the software SAINT+,[69] and absorption effects were corrected by the multi-scan method implemented in SADABS.[70] The structure was solved using SHELXTL incorporated in the Bruker APEX-III software package and refined through SHELXLE and PLATON programs.[71,72] All the non-hydrogen atoms of the structures were successfully refined using anisotropic displacement parameters. H-atoms bound to carbon atoms were placed at geometrical positions using suitable HFIX instructions in SHELXL and included in subsequent refinement cycles in riding-motion approximation with isotropic thermal displacement parameters (U_{iso}) fixed at the carbon atom to which they are attached. Some electron density was found in the data of the crystal structure, probably due to additional disordered solvent molecules occupying the spaces created by the packing arrangement of the cluster compound. Efforts to accurately locate, model and refine these residues were ineffective, and the investigation of the total potential solvent area using the software package PLATON[73,74] confirmed the existence of cavities with potential solvent accessible void volume. Thus, the original data sets were treated with the program SQUEEZE,[75] which is used to calculate the contribution of the smeared electron density in the lattice voids and adds this to the calculated structure factors from the structural model when refining against the *hkl* file.

Various figures of the structures were created, using Diamond 3 and Mercury software packages.[76,77] Additional structural drawings of the four complexes with thermal ellipsoids at 50% probability are shown in Fig. S9.† The unit cell parameters, structure solution, and refinement details of **1**, **2**, **3**·2MeOH, and **4**·2CH$_2$Cl$_2$ are summarized in Table S8.† Further crystallographic details can be found in the corresponding CIF files provided in the ESI.†

Conflicts of interest

There are no conflicts to declare.

Acknowledgements

References

1 D. Gatteschi, R. Sessoli and J. Villain, *Molecular Nanomagnets*, Oxford University Press, Oxford, MS, USA, 2006.

2 M. Atzori and R. Sessoli, *J. Am. Chem. Soc.*, 2019, **141**, 11339.

3 For representative reviews, see: (*a*) R. Bagai and G. Christou, *Chem. Soc. Rev.*, 2009, **38**, 1011; (*b*) C. J. Milios and R. E. P. Winpenny, *Struct. Bonding*, 2015, **164**, 1.

4 F. Habib and M. Murugesu, *Chem. Soc. Rev.*, 2013, **42**, 3278.

5 (*a*) J. M. Frost, K. L. M. Harriman and M. Murugesu, *Chem. Sci.*, 2016, **7**, 2470–2491; (*b*) M. Feng and M.-L. Tong, *Chem. – Eur. J.*, 2018, **24**, 7574.

6 M. J. Heras Ojea, L. C. H. Maddock and R. A. Layfield, Lanthanide Organometallics as Single-Molecule Magnets, in *Organometallic Magnets. Topics in Organometallic Chemistry*, ed. V. Chandrasekhar and F. Pointillart, Springer, Cham, 2019, vol. 64.

7 C. Papatriantafyllopoulou, E. E. Moushi, G. Christou and A. J. Tasiopoulos, *Chem. Soc. Rev.*, 2016, **45**, 1597.

8 A. M. Ako, I. J. Hewitt, V. Mereacre, R. Clerac, W. Wernsdorfer, C. E. Anson and A. K. Powell, *Angew. Chem., Int. Ed.*, 2006, **45**, 4926.

9 C. J. Milios, A. Vinslava, W. Wernsdorder, S. Moggach, S. Parsons, S. P. Perlepes, G. Christou and E. K. Brechin, *J. Am. Chem. Soc.*, 2006, **129**, 2754.

10 Th. C. Stamatatos, D. Foguet-Albiol, S.-C. Lee, C. C. Stoumpos, C. P. Raptopoulou, A. Terzis, W. Wernsdorfer, S. O. Hill, S. P. Perlepes and G. Christou, *J. Am. Chem. Soc.*, 2007, **129**, 9484.

11 For a very recent review, see: P. Konieczny, W. Sas, D. Czernia, A. Pacanowska, M. Fitta and R. Pełka, *Dalton Trans.*, 2022, **51**, 12762.

12 F.-S. Guo, B. M. Day, Y.-C. Chen, M.-L. Tong, A. Mansikkamäki and R. A. Layfield, *Science*, 2018, **362**, 1400.

13 N. F. Chilton, *Inorg. Chem.*, 2015, **54**, 2097.

14 J. Tang and P. Zhang, *Lanthanide Single Molecule Magnets*, Springer-Verlag, Heidelberg, Germany, 2015.

15 L. Bogani and W. Wernsdorfer, *Nat. Mater.*, 2008, **7**, 179.

16 D. Aguilà, L. A. Barrios, V. Velasco, O. Roubeau, A. Repollés, P. J. Alonso, J. Sesé, S. J. Teat, F. Luis and G. Aromí, *J. Am. Chem. Soc.*, 2014, **136**, 14215.

17 M. Ganzhorn, S. Klyatskaya, M. Ruben and W. Wernsdorfer, *ACS Nano*, 2013, 7, 6225.

18 P. Zhang, Y.-N. Guo and J. Tang, *Coord. Chem. Rev.*, 2013, **257**, 1728.

19 Z. Zhu, M. Guo, X.-L. Li and J. Tang, *Coord. Chem. Rev.*, 2019, **378**, 350.

20 J. D. Rinehart and J. R. Long, *Chem. Sci.*, 2011, **2**, 2078.

21 E. Moreno-Pineda, G. Taran, W. Wernsdorfer and M. Ruben, *Chem. Sci.*, 2019, **10**, 5138.

22 J.-L. Liu, Y.-C. Chen and M.-L. Tong, *Chem. Soc. Rev.*, 2018, **47**, 2431.

23 K. S. Pedersen, D. N. Woodruff, J. Bendix and R. Clérac, in *Lanthanides and Actinides in Molecular Magnetism*, ed. R. A. Layfield and M. Murugesu, Wiley-VCH, Berlin, Germany, 1st edn, 2015, pp. 125–152.

24 Y. Gil, A. Castro-Alvarez, P. Fuentealba, E. Spodine and D. Aravena, *Chem. – Eur. J.*, 2022, **28**, e202200336.

25 P. Zhang, L. Zhang and J. Tang, *Curr. Inorg. Chem.*, 2013, **3**, 101.

26 For example, see: (*a*) J. Zhang, Z. Zhang, Z. Chen and X. Zhou, *Dalton Trans.*, 2012, **41**, 357; (*b*) H. Tian, B.-L. Wang, J. Lu, H.-T. Liu, J. Su, D. Li and J. Dou, *Chem. Commun.*, 2018, **54**, 12105; (*c*) T. Bereta, A. Mondal, K. Ślepokura, Y. Peng, A. K. Powell and J. Lisowski, *Inorg. Chem.*, 2019, **58**, 4201.

27 For example, see: (*a*) M. Guo, Y. Xu, J. Wu, L. Zhao and J. Tang, *Dalton Trans.*, 2017, **46**, 8252; (*b*) C. P. Burns, B. O. Wilkins, C. M. Dickie, T. P. Latendresse, L. Vernier, K. R. Vignesh, N. S. Bhuvanesh and M. Nippe, *Chem. Commun.*, 2017, **53**, 8419; (*c*) M. Guo, Y.-Q. Zhang, Z. Zhu and J. Tang, *Inorg. Chem.*, 2018, **57**, 12213; (*d*) F. Pointillart, B. Le Guennic, S. Golhen, O. Cador and L. Ouahab, *Chem. Commun.*, 2013, **49**, 11632.

28 V. S. Sastri, J. R. Perumareddi, V. Ramachandra Rao, G. V. S. Rayudu and J.-C. Bunzli, in *Modern Aspects of Rare Earths and their Complexes*, 1st edn, 2003.

29 S. Xue, L. Zhao, Y.-N. Guo, R. Deng, Y. Guo and J. Tang, *Dalton Trans.*, 2011, **40**, 8347.

30 C. Pelizzi, G. Pelizzi, G. Predieri and S. Resola, *J. Chem. Soc., Dalton Trans.*, 1982, 1349.

31 C. Pelizzi, G. Pelizzi and F. Vitali, *Transition Met. Chem.*, 1986, **11**, 401.

32 D. Delledonne, G. Pelizzi and C. Pelizzi, *Acta Crystallogr., Sect. C: Cryst. Struct. Commun.*, 1987, **43**, 1502.

33 A. Bonardi, S. Ianelli, C. Pelizzi and G. Pelizzi, *Inorg. Chim. Acta*, 1991, **187**, 167.

34 I. Mylonas-Margaritis, D. Maniaki, J. Mayans, L. Ciammaruchi, V. Bekiari, C. P. Raptopoulou, V. Psycharis, S. Christodoulou, A. Escuer and S. P. Perlepes, *Magnetochemistry*, 2018, **4**, 45.

35 E. Pilichos, I. Mylonas-Margaritis, A. P. Kontos, V. Psycharis, N. Klouras, C. P. Raptopoulou and S. P. Perlepes, *Inorg. Chem. Commun.*, 2018, **94**, 48.

36 W. Harhouri, C. Mchiri, S. Najmudin, C. Bonifácio and H. Nasri, *Acta Crystallogr., Sect. E: Crystallogr. Commun.*, 2016, **72**, 720.

37 K. Nakamoto, *Infrared and Raman Spectra of Inorganic and Coordination Compounds*, Wiley, New York, NY, USA, 4th edn, 1986.

38 (*a*) G. B. Deacon and R. J. Phillips, *Coord. Chem. Rev.*, 1980, **33**, 227; (*b*) D. Martinez, M. Motevalli and M. Watkinson, *Dalton Trans.*, 2010, 446.

39 V. Zeleňák, Z. Vargová and K. Györyová, *Spectrochim. Acta, Part A*, 2007, **66**, 262.

40 X. Sun, Y.-K. Yang and F. Lu, *Macromolecules*, 1998, **31**, 4291.

41 M. Llunell, D. Casanova, J. Girera, P. Alemany and S. Alvarez, *SHAPE, Continuous Shape Measures Calculation; Version 2.0*, Universitat de Barcelona, Barcelona, Spain, 2010.

42 (*a*) A. K. Bar, P. Kalita, J.-P. Sutter and V. Chandrasekhar, *Inorg. Chem.*, 2018, **57**, 2398; (*b*) P. Rey, A. I. Smolentsev and K. E. Vostrikova, *Molecules*, 2022, **27**, 1626; (*c*) B.-Y. Chen, M.-Y. Tsai, Y.-C. Su, P.-H. Lin and J. Long, *CrystEngComm*, 2021, **23**, 8343.

43 For an excellent paper discussing N–H⋯Cl hydrogen bonds, see: J. V. Gavette, C. M. Klug, L. N. Zakharov, M. P. Shores, M. M. Haley and D. W. Johnson, *Chem. Commun.*, 2014, **50**, 7173.

44 (*a*) P. Antal, B. Drahoš, R. Herchel and Z. Trávníček, *Dalton Trans.*, 2016, **45**, 15114; (*b*) L. Mandal, S. Biswas and M. Yamashita, *Magnetochemistry*, 2019, **5**, 56.

45 E. C. Manickas, M. Zeller and C. M. Zaleski, *Acta Crystallogr., Sect. E: Crystallogr. Commun.*, 2020, **76**, 1213.

46 For example, see: (*a*) G. Abbas, Y. Lan, G. E. Kostakis, W. Wernsdorfer, C. E. Anson and A. K. Powell, *Inorg. Chem.*, 2010, **49**, 8067; (*b*) Y.-X. Zhang, Y.-H. Zhang, B.-Y. Liu, W.-M. Wang, G.-P. Tang, H.-Y. Wei and Z.-L. Wu, *New J. Chem.*, 2018, **42**, 18305; (*c*) K. Zhang, G.-P. Li, V. Montigaud, O. Cador, B. Le Guennic, J. Tang and Y.-Y. Wang, *Dalton Trans.*, 2019, **48**, 2135; (*d*) H. Ke, P. Gamez, L. Zhao, G.-F. Xu, S. Xue and J. Tang, *Inorg. Chem.*, 2010, **49**, 7549.

47 G. G. Morgan and I. A. Kühne, in *Practical Approaches to Biological Inorganic Chemistry*, ed. R. R. Crichton and R. O. Louro, 2nd edn, 2020, pp. 69–119.

48 For an excellent comprehensive review, see: D. N. Woodruff, R. E. P. Winpenny and R. A. Layfield, *Chem. Rev.*, 2013, **113**, 5110.

49 T. G. Ashebr, H. Li, X. Ying, X.-L. Li, C. Zhao, S. Liu and J. Tang, *ACS Mater. Lett.*, 2022, **4**, 307.

50 Z. Zhu, C. Zhao, T. Feng, X. Liu, X. Ying, X.-L. Li, Y.-Q. Zhang and J. Tang, *J. Am. Chem. Soc.*, 2021, **143**, 10077.

51 (*a*) D. I. Alexandropoulos, A. A. Alaimo, D. Sun and Th. C. Stamatatos, *Magnetochemistry*, 2018, **4**, 48; (*b*) E. C. Mazarakioti, J. Regier, L. Cunha-Silva, W. Wernsdorfer, M. Pilkington, J. Tang and Th. C. Stamatatos, *Inorg. Chem.*, 2017, **56**, 3568; (*c*) K. N. Pantelis, P. S. Perlepe, S. Grammatikopoulos, C. Lampropoulos, J. Tang and Th. C. Stamatatos, *Molecules*, 2020, **25**, 2191.

52 Y.-N. Guo, G.-F. Xu, W. Wernsdorfer, L. Ungur, Y. Guo, J. Tang, H.-J. Zhang, L. F. Chibotaru and A. K. Powell, *J. Am. Chem. Soc.*, 2011, **133**, 11948.

53 S. T. Liddle and J. van Slageren, *Chem. Soc. Rev.*, 2015, **44**, 6655.

54 For example, see: (*a*) Z. Zhu, C. Zhao, T. Feng, X. Liu, X. Ying, X.-L. Li, Y.-Q. Zhang and J. Tang, *J. Am. Chem. Soc.*, 2021, **143**, 10077; (*b*) Z.-H. Li, Y.-Q. Zhai, W.-P. Chen, Y.-S. Ding and Y.-Z. Zheng, *Chem. – Eur. J.*, 2019, **25**, 16219; (*c*) A. B. Canaj, S. Dey, E. R. Martí, C. Wilson, G. Rajaraman and M. Murrie, *Angew. Chem., Int. Ed.*, 2019, **58**, 14146.

55 (*a*) J. Li, S. Gómez-Coca, B. S. Dolinar, L. Yang, F. Yu, M. Kong, Y.-Q. Zhang, Y. Song and K. R. Dunbar, *Inorg. Chem.*, 2019, **58**, 2610; (*b*) B. Ali, X.-L. Li, F. Gendron, B. Le Guennic and J. Tang, *Dalton Trans.*, 2021, **50**, 5146.

56 L. I. Semenova and A. H. White, *Aust. J. Chem.*, 1999, **52**, 571.

57 K. S. Cole and R. H. Cole, *J. Chem. Phys.*, 1941, **9**, 341.

58 Y.-N. Guo, G.-F. Xu, Y. Guo and J. Tang, *Dalton Trans.*, 2011, **40**, 9953.

59 For example, see: (*a*) N. Qiao, X.-X. Li, Y. Chen, X.-Y. Xin, C. Yang, S.-S. Dong, Y.-Z. Wang, X.-J. Li, Y.-P. Hua and W.-M. Wang, *Polyhedron*, 2022, **215**, 115675; (*b*) Y. Peng, V. Mereacre, C. E. Anson and A. K. Powell, *Inorganics*, 2016, **4**, 2; (*c*) J. Wang, Z.-L. Wu, L.-R. Yang, M.-M. Xue, Z.-X. Fang, S.-C. Luo and W.-M. Wang, *Inorg. Chim. Acta*, 2021, **514**, 120015; (*d*) J. Wu, X.-L. Li, L. La Droitte, O. Cador, B. Le Guennic and J. Tang, *Dalton Trans.*, 2021,

50, 15027; (*e*) M. U. Anwar, A. Al-Harrasi, J. M. Rawson, E. L. Gavey, J. Regier, D. Alexandropoulos, M. Pilkington and L. K. Thompson, *Dalton Trans.*, 2019, **48**, 14269.

60 C. Pelizzi and G. Pelizzi, *Acta Crystallogr., Sect. B: Struct. Crystallogr. Cryst. Chem.*, 1979, **35**, 126.

61 G. A. Bain and J. F. Berry, *J. Chem. Educ.*, 2008, **85**, 532.

62 *CrystalClear*, Rigaku/MSC Inc., The Woodlands, TX, USA, 2005.

63 G. M. Sheldrick, *Acta Crystallogr., Sect. A: Fundam. Crystallogr.*, 2008, **64**, 112.

64 G. M. Sheldrick, *Acta Crystallogr., Sect. C: Cryst. Struct. Commun.*, 2015, **71**, 3.

65 A. L. Spek, *Acta Crystallogr., Sect. C: Cryst. Struct. Commun.*, 2015, **71**, 9.

66 O. V. Dolomanov, L. J. Bourhis, R. J. Gildea, J. A. K. Howard and H. Puschmann, *J. Appl. Crystallogr.*, 2009, **42**, 339.

67 T. Kottke and D. Stalke, *J. Appl. Crystallogr.*, 1993, **26**, 615.

68 *APEX2. Data Collection Software Version 2012.4*, Bruker AXS, Delft, The Netherlands, 2012.

69 *SAINT+, Data Integration Engine v. 7.23a ©*, Bruker AXS, Madison, Wisconsin, USA, 1997–2005.

70 G. M. Sheldrick, *SADABS v.2.01, Bruker/Siemens Area Detector Absorption Correction Program*, Bruker AXS, Madison, Wisconsin, USA, 1998.

71 *APEX-III*, Bruker AXS Inc., Madison, Wisconsin, USA, 2016.

72 C. B. Hübschle, G. M. Sheldrick and B. Dittrich, *J. Appl. Crystallogr.*, 2011, **44**, 1281.

73 A. L. Spek, *Acta Crystallogr., Sect. A: Found. Crystallogr.*, 1990, **46**, C34.

74 A. L. Spek, *J. Appl. Crystallogr.*, 2003, **36**, 7.

75 P. Van der Sluis and A. L. Spek, *Acta Crystallogr., Sect. A: Found. Crystallogr.*, 1990, **46**, 194.

76 K. Bradenburg, *DIAMOND, Release 3.1f*, Crystal Impact GbR, Bonn, Germany, 2008.

77 I. J. Bruno, J. C. Cole, P. R. Edgington, M. K. Kessler, C. F. Macrae, P. McCabe, J. Pearson and R. Taylor, *Acta Crystallogr., Sect. B: Struct. Sci.*, 2002, **58**, 389.